IEEE Access
Multidisciplinary | Rapid Review | Open Access Journal

Received August 2, 2020, accepted August 19, 2020, date of publication August 24, 2020, date of current version September 4, 2020.

Digital Object Identifier 10.1109/ACCESS.2020.3019197

A Fast and Efficient Maximum Power Tracking Combining Simplified State Estimation With Adaptive Perturb and Observe

SHUN-CHUNG WANG[1], HUNG-YU PAI[2], GUAN-JHU CHEN[2], (Student Member, IEEE), AND YI-HWA LIU[2], (Member, IEEE)

[1]Department of Electrical Engineering, Lunghwa University of Science and Technology, Taoyuan 33306, Taiwan
[2]Department of Electrical Engineering, National Taiwan University of Science and Technology, Taipei 10607, Taiwan

Corresponding author: Shun-Chung Wang (wangsc@mail.lhu.edu.tw)

This work was supported in part by the Ministry of Science and Technology, Taiwan, under Grant MOST 109-2221-E-262-001.

ABSTRACT This paper proposes a fast and efficient maximum power tracking approach, which synthesizes simplified model-based state estimation (SMSE) with adaptive alpha perturb-and-observe (α-P&O) method, to further raise the capability and efficacy of maximum power point (MPP) tracking (MPPT). Only any two sampling points, in the first stage, on the operating characterization curve are needed to estimate the irradiance and temperature based on SMSE. In the second phase, the operation point is moved directly to the operating voltage command (OVC) derived from the fitting relationship between the voltages at MPP under various insolation intensities, and then the α-P&O method takes over the next tracking to pinpoint the exact MPP. Performances are demonstrated through simulations and experiments. Experimental results reveal that tracking accuracies exceed 99.2 % in all test scenarios. Comparing with conventional and variable step-size P&O methods, the tracking time is shortened by 84.6 % and 76.0 %, improvement of 1.26 % and 0.03 % in tracking accuracy can also be achieved, and the tracking energy loss is reduced by 68.0 % and 52.7 %, respectively.

INDEX TERMS Maximum power point tracking, photovoltaic generation system, perturb and observe, state estimation.

I. INTRODUCTION

The photovoltaic (PV) generation system (PGS) has gained popularity in the worldwide electricity market in recent years since the solar energy is clean, abundant, sustainable, and environmental friendly [1], [2]. Technologies adopted to extract the maximum available power from PV modules is one of the essential parts in the existing PGS due to the low photoelectric conversion efficiency. Besides, the generated electricity of the PGS is relevant to the electrical characteristics of solar cells and dominated by the intensity of solar irradiance and temperature. An efficient and simple MPPT technique can achieve optimum utilization of the solar energy in steady state, but there will be certain amount of energy loss if the power tracker fails to reach the MPP within a short duration. As a result, further development of effective MPPT approaches with fast tracking speed and low tracking loss is indispensable to a PGS for long-term planning and deployment [3]–[5].

In the past two decades, a variety of MPPT techniques have been proposed in numerous literatures. Most of the studied methods can successfully accomplish what they claim under stable atmospheric conditions. Among them, the P&O method, the hill climbing (HC) method [6]–[8] and the incremental conductance (INC) method [9], are the methods used widely owing to the simplicity and ease of implementation. Previous studies report that the conventional P&O method exists a trade-off for the tracking time and accuracy, and the determination of an appropriate perturbation step size (SS) for optimizing the tracking performance is very critical and challenging. Besides, conventional P&O and INC methods suffer drift problem under fast changing atmospheric conditions. To deal with these problems, three categories of tracking technologies were proposed [10]: 1) variable step

The associate editor coordinating the review of this manuscript and approving it for publication was Lorenzo Ciani.

size (VSS) MPPT methods, 2) hybrid MPPT methods, and 3) MPPT methods based on PV mathematical model.

In the first category, multiplying the SS by a reduction or scaling factor when the operating point (OP) passes through the MPP is proposed in [11] to achieve fast tracking purpose. The SS in [12] takes the absolute value of the solar array power derivative to multiply its exponent of output power. Although the aforementioned methods can solve the trade-off problem, an optimal scaling factor is still hard to obtain.

For the second category, these MPPT methods comprise two or more algorithms. One algorithm was adopted to identify the probable region of the true MPP located and the actual MPP was pinpointed using the other algorithms. A new MPPT algorithm combining the particle swarm optimization (PSO) with the conventional P&O method was presented in [13]. An improved MPPT method was proposed in [14], it blends the adaptive P&O and the PSO with the search-skip-judge mechanism to minimize the searching region within the P-V curve and make faster convergence attainable. A PSO augmented Internet of Things based MPPT method is proposed in [15], which exhibits better performance over P&O, PSO, ant colony optimization, and artificial bee colony MPPT techniques. The hybrid MPPT technology does not require precise PV models, but the manipulation in the first-stage tracking process is still complicated.

Model-based MPPTs have been proposed in the third category to enhance the tracking performances. Excluding the measurements of the temperature and irradiance, the MPP can be analytically determined based on the PV mathematical model and the parameter data were supplied by manufacturers. Teng *et al.* [16] proposed a model-based parameter estimation method to estimate the irradiance level and temperature, and then calculates the actual MPP position using these obtained values. A combined MPPT technique featuring the fast tracking of the typical model-based techniques and the low steady-state error provided by the heuristic techniques was proposed in [17]. Cristaldi *et al.* [18] devised an improved model-based MPPT technique that does not need expensive irradiance sensors. The irradiance was estimated by a numerical solver using the inverse PV model based on the measurements of the panel voltage, current, and temperature.

In addition to standalone PGS, MPPT techniques can also be applied to grid-integrated PV systems [19]–[22], hybrid renewable energy systems [23]–[26], PV water pumping system [27], [28] and Internet of Things [15]. In [19]–[22], fuzzy particle swarm optimization MPPT method [19], modified sine-cosine optimized algorithm [20], hybrid adaptive neuro-fuzzy inference system and artificial bee colony algorithm [21], and adaptive neuro-fuzzy inference system–particle swarm optimization-based hybrid MPPT technique [22] have been successfully applied to grid-integrated PV systems to achieve fast convergence and high accuracy. In [23]–[26], a firefly asymmetrical fuzzy logic controller based unified MPPT hybrid controller, hybrid fuzzy particle swarm optimization-based MPPT approach, Jaya-based MPPT method, and Lyapunov controller are utilized in PV-Wind-Fuel Cell hybrid system [23], hybrid PV-wind system [24] and PV-Fuel Cell systems [25], [26] to achieve high efficiency and stable operation. Besides, hybrid artificial neural network-fuzzy logic control tuned flower pollination algorithm [27] and hybrid gravitational search algorithm-particle swarm optimization based MPPT method [28] are adopted for MPP tracking in PV water pumping systems.

This paper proposes a fast two-phase MPPT method, which combines simplified model-based state estimation (SMSE) with α-P&O method, to improve the performance of MPP tracking. By measuring the voltage-and-current sets of any two OPs, the solar irradiance and temperature can be estimated by the SMSE. Using these obtained values, an operating voltage command (OVC) close to the MPP is calculated via a polynomial derived from the power versus voltage characteristic curves. In the second stage, the operation point is moved to the obtained OVC, and the α-P&O takes over the MPP tracking and mitigates the oscillation power loss in the following processes. The proposed method features fast dynamic response during the first stage and low steady-state power loss in the second phase. The main contribution of this study is that the swift and accurate tracking can be attained without the need of extra and costly irradiance and temperature sensors, and the easy integration with the conventional P&O method. Based on the current research results, the proposed method is specifically suitable for manipulating rapid MPP tracking under non-partial shading conditions. The rest of this paper is organized as follows: Section II starts with an overview of the PV model used. Then, the philosophy of the proposed method is explained and derived systematically in Section III. In Section IV, the simulation and experimental tests are carried out and the results are compared with earlier techniques to demonstrate the effectiveness. Finally, Section V concludes this paper.

II. MODEL OF PV MODULE

Several mathematical models of the PV cell have been studied in the literature. Differences between these proposed PV models are their complexity and the degree of details modeled. Single-diode equivalent circuit model based on the macroscopic characteristic is one of the most extensively adopted owing to its compromise between accuracy and simplicity in numerous applications [29]. Fig. 1 illustrates the single-diode equivalent circuit of a PV solar cell. The relationship between the terminal current (I_T) and voltage (V_T) of a PV module, from Fig. 1, can be expressed by

$$I_T = I_g - I_s\left(e^{\frac{q(R_S I_T + V_T)}{KATN}} - 1\right) - \frac{R_S I_T + V_T}{R_P} \tag{1}$$

where q, K, T and N are the electron charge ($1.602 \times 10^{-19} C$), Boltzmann constant ($1.38065 \times 10^{-23} J/K$), panel temperature in Kelvin, and number of cells connected in series, respectively. The five parameters, I_g, I_s, A, R_S and R_P, are the photoelectric current for a certain solar irradiation S (W/m^2), reverse saturation current, diode ideality factor,

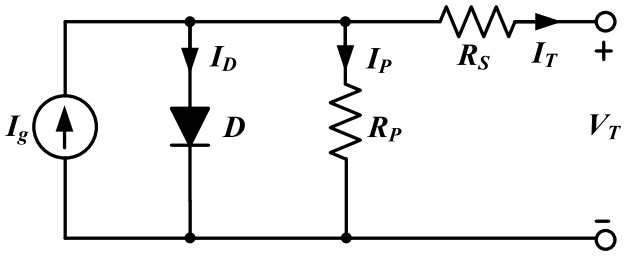

FIGURE 1. Equivalent circuit of a PV solar cell.

and equivalent series and shunt resistances, respectively. The I_g generated by a certain solar irradiation S can be represented by

$$I_g = \frac{S}{1000} \times I_{SC} \tag{2}$$

where I_{SC} stands for the short-circuit current of the PV module at the irradiance 1000W/m^2. The equivalent shunt resistance is much larger than the series resistance, and the R_S is small. Then, from (1) and (2), a concise form can be expressed as function of $I_T = f(V_T, S, T)$ by neglecting the R_P and R_S to simplify (1), which can be given by

$$I_T\,(V_T, S, T) = \frac{S}{1000} \times I_{SC} - I_s\left(e^{\frac{qV_T}{KATN}} - 1\right) \tag{3}$$

Hence, the output power of the PV module can be obtained via the terminal voltage multiplied by the terminal current. Based on (3) under different irradiative intensities and temperatures, the power versus voltage (P-V) curves of the studied PV module TYNS62610290 from Tynsolar Corp. connected in 2-series-1-parallel (expressed as 2S1P) can be plotted in Fig. 2(a) and (b), respectively.

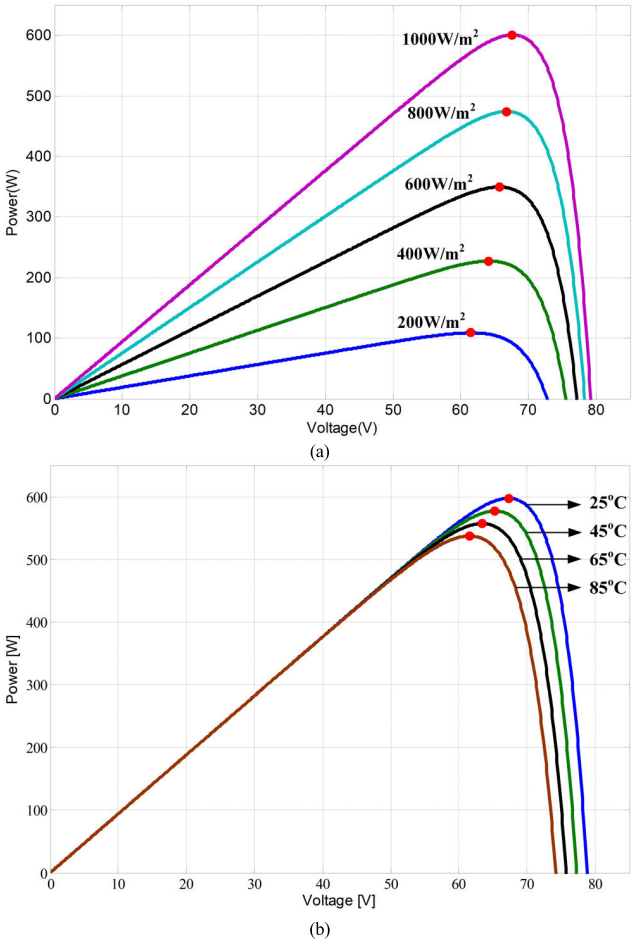

FIGURE 2. P-V curves of solar module. (a) Under different irradiances (T = 25°C). (b) Under different temperatures (S = 1000 W/m^2).

III. PHILOSOPHY OF PROPOSED MPPT METHOD

A novel two-stage MPPT method is proposed in this paper by integrating the SMSE with α-P&O method. Only two sampling OPs are needed to estimate the current solar irradiance through SMSE. Then, an OVC close to the MPP is computed via the fitted curve between the irradiance intensities and the MPP voltages. Next, the operation point will be moved to the calculated OVC, and the α-P&O takes over to harvest the MPP precisely. The following subsections will introduce the proposed simplified model-based state estimation, as well as the philosophy and operating mechanism of the proposed two-stage tracking technique.

A. SIMPLIFIED MODEL-BASED STATE ESTIMATION

The fundamental of the state estimation (SE) is that every other quantity about the system can be calculated from the known system state. i.e., the system parameters wanted to know can be obtained through the time history of measurements and system function. The common approach utilized to solve the SE is the weighted least square (WLS) technique [30]. For example, referring to the MPPT problem studied in this paper, the irradiance level (S) and temperature (T) are considered as system parameters which are to be known. The measured voltages and currents of the OPs at different time periods and the characteristic curves of the PGS are the time history of measurements and system functions, respectively. Hence, it can be seen from (3) that provided the two values of the I_T and V_T were measured, then both S and T can be figured out. In other words, the intensities of irradiance and temperature can be obtained by solving (4) iteratively [30]. Through iterations the system parameters can be estimated until the mismatch vector $[\Delta S \Delta T]$ converges to a constraint default.

$$\begin{bmatrix} \Delta S_j \\ \Delta T_j \end{bmatrix} = ([H_j]^T [W_j][H_j])^{-1}[H_j]^T [W_j][\Delta I_j] \tag{4a}$$

$$\begin{bmatrix} S_{j+1} \\ T_{j+1} \end{bmatrix} = \begin{bmatrix} S_j \\ T_j \end{bmatrix} + \begin{bmatrix} \Delta S_j \\ \Delta T_j \end{bmatrix} \tag{4b}$$

In this study, the estimation is achieved by measuring any two different voltage-and-current sets (I_1, V_1) and (I_2, V_2) on the P-V curve. Consequently, the mismatch vector of current, $[\Delta I_j]$, weighting vector $[W_j]$, and the Jacobian matrix $[H_j]$ for the j^{th} iteration process can be expressed by

$$[\Delta I_j] = \begin{bmatrix} I_{T1}(S_j, T_j, V_1) - I_1 \\ I_{T2}(S_j, T_j, V_2) - I_2 \end{bmatrix} = \begin{bmatrix} \Delta I_{1,j} \\ \Delta I_{2,j} \end{bmatrix} \tag{5a}$$

TABLE 1. Simulation results of WLS-based SE.

Index \ No.	1	2	3	4*
S (W/m^2)	1000.03	1000.00	1000.00	1000.00
T (K)	292.93	297.8	297.99	298

$$[W_j] = \begin{bmatrix} W_1 & 0 \\ 0 & W_2 \end{bmatrix} \tag{5b}$$

$$[H_j] = \begin{bmatrix} \dfrac{\partial I_{T1}(S_j, T_j, V_1)}{\partial S} & \dfrac{\partial I_{T1}(S_j, T_j, V_1)}{\partial T} \\ \dfrac{\partial I_{T2}(S_j, T_j, V_2)}{\partial S} & \dfrac{\partial I_{T2}(S_j, T_j, V_2)}{\partial T} \end{bmatrix} = \begin{bmatrix} H_{11,j} & H_{12,j} \\ H_{21,j} & H_{22,j} \end{bmatrix} \tag{5c}$$

However, the complexity of the aforementioned WLS-based SE is complicated, and it is difficult to be realized using low-cost microcontroller units (MCUs). In addition, the correctness of the estimation depends to a large extension on the quality of measurement and the accuracy of the system parameters. Furthermore, the SE may fail to converge toward a solution even when it exists if the measurement error is too large. Therefore, a simplified model based state estimation method is proposed in this study.

A simulation based on WLS-based SE was performed and the obtained results is shown in Table 1. From Table 1, the initial conditions of $S = 800$ W/m^2 and $T = 323$K are guessed to start the estimation, and the target values are 1000 W/m^2 and 298K respectively. From Table 1, four iterations are needed to meet the convergence criterion, and it should be noted that the irradiance has almost been correctly estimated at the first round of estimation in spite of a small error exists in the temperature still.

To reduce the computation complexity and deal with the convergence problem of WLS-based SE, a SMSE is proposed herein. The conventional WLS-based SE is simplified as only one estimation run. Because only one estimation run is required, the updated mechanisms can be rewritten as

$$S_{fe} = S_g + \frac{1}{D} \times H_{22,1} \times \Delta I_{1,f} - \frac{1}{D} \times H_{12,f} \times \Delta I_{2,f} \tag{6a}$$

$$T_{fe} = T_g - \frac{1}{D} \times H_{21,1} \times \Delta I_{1,f} + \frac{1}{D} \times H_{11,f} \times \Delta I_{2,f} \tag{6b}$$

where D is the norm of the Jacobian matrix, it is given by

$$D = H_{11,f} \times H_{22,f} - H_{12,f} \times H_{21,f} \tag{7}$$

In (6), the S_{fe} and T_{fe} are the estimated values at the first time, and the S_g and T_g are the guessed initial values. Besides, the Jacobian matrix and current error vector in SMSE method can be denoted respectively as

$$[H_f] = \begin{bmatrix} \dfrac{\partial I_{T1}(S_g, T_g, V_1)}{\partial S} & \dfrac{\partial I_{T1}(S_g, T_g, V_1)}{\partial T} \\ \dfrac{\partial I_{T2}(S_g, T_g, V_2)}{\partial S} & \dfrac{\partial I_{T2}(S_g, T_g, V_2)}{\partial T} \end{bmatrix} = \begin{bmatrix} H_{11,f} & H_{12,f} \\ H_{21,f} & H_{22,f} \end{bmatrix} \tag{8a}$$

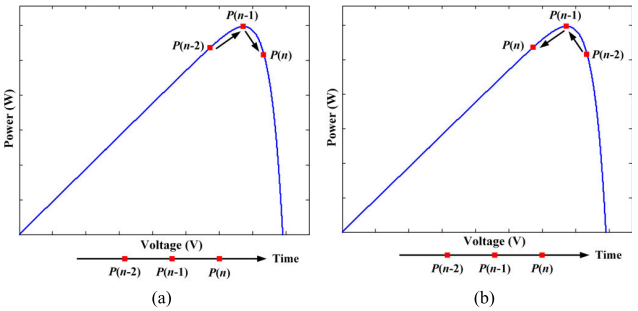

FIGURE 3. Tracking route. (a) Start from short-circuit current end. (b) Start from open-circuit voltage end.

$$[\Delta I_f] = \begin{bmatrix} I_{T1}(S_g, T_g, V_1) - I_1 \\ I_{T2}(S_g, T_g, V_2) - I_2 \end{bmatrix} = \begin{bmatrix} \Delta I_{1,f} \\ \Delta I_{2,f} \end{bmatrix} \tag{8b}$$

B. THE α-P&O METHOD

There are many literatures have proposed a variety of VSS P&O methods to improve the problem of steady-state oscillation near the MPP occurring in the fixed-step P&O method. However, the more parameters involved in these methods, the more complicated the computations required. Therefore, based on the essence of the VSS P&O, the α-P&O method that we first proposed in [31] is adopted in this study. The α-P&O method initially uses the maximum possible perturbation SS. When the OP passes the MPP, the proposed method reverses the tracking direction and multiplies the perturbation SS by a scaling factor α to reduce the step size, as shown in (9)

$$\Delta V(n) = \alpha \cdot \Delta V(n-1) \tag{9}$$

where $\Delta V(n)$ is the current voltage perturbation, $\Delta V(n\text{-}1)$ is the previous voltage disturbance. Equation (9) is very simple. In order to effectively reduce the steady-state oscillation, the α must be selected to be less than 1. On the other hand, to ensure that the system has swift dynamic response, the detected power needs to meet the following criterion before equation (9) can be applied:

$$P(n-2) < P(n-1) \;\&\&\; P(n-1) > P(n) \tag{10}$$

where $P(n)$ stands for current power value, $P(n\text{-}1)$ is the power value of the previous sampling, and $P(n\text{-}2)$ denotes the power value of the sampling previous to $P(n\text{-}1)$. The execution criterion setting for the α-P&O algorithm, as illustrated in Fig. 3, makes the MPP tracking attainable with high steady-state accuracy regardless of whether the tracking route is started from the short-circuit current end or the open-circuit voltage end of the P-V curve. In addition, the OP in the next tracking process is directly moved to the OVC figured out based on the irradiance estimated in the prior stage, which is close to the MPP essentially. Then, the α-P&O algorithm takes over the subsequent tracking and continuously perturbs around the MPP. As a result, the SS in (9) will rapidly decrease until the minimum step ΔV_{min} allowed by the system is reached.

Within the range of 0 to 1 (excluding 0 and 1), the value of α can be selected arbitrarily. If the α is significantly smaller than 1, then the step size will be reduced considerably when the OP passes the MPP. However, when the distance between the OP and the MPP is substantial after the OP passes MPP, then using a small SS requires a large number of perturbations for the OP to pass the MPP again. Conversely, if α approximates 1, fewer numbers of steps are required for the OP to pass the MPP again; however, the magnitude of the step-size reduction declines considerably each time when the OP passes the MPP. To implement the proposed tracking strategy using a low-cost MCU, the minimum and maximum values of α are set to (1/16) and (15/16) respectively, and a step change of the α value is (1/16). The main reason is that when α is in this format, equation (9) can be executed simply by the operations of right shift and addition, which can improve the computational complexity. In the case studied, after extensive simulation and testing under different values of α, the results indicate that the 8/16 has a competitively good effect on decreasing the number of tracking steps required and the tracking time. Therefore, the α is specified as 0.5 in this paper.

C. PROPOSED MPPT TECHNIQUE

Fig. 4 illustrates the conceptual scheme of the proposed MPPT approach. In Fig. 4, V_1 and V_2 are any two operating points which are measured first to estimate the current irradiation intensity. Once the irradiant level is known using (6), an OVC close to the MPP at current irradiation level (i.e. the voltage at "a" or "c") can be obtained by a fitted curve, which will be explained later. In the next step, the OP is directly moved to the "a" or "c" point, and then the α-P&O method is in charge of the tracking procedure to chase the MPP. During the α-P&O cycle, the OP will move alternately among the a, b, and c three points, and the perturbation SS will gradually decrease so that an exact MPP can be located. In this study, the various sampling positions of V_1 and V_2 on the P-V curve have been tried through comprehensive simulation, the studied algorithm can converge to achieve high-accuracy tracking for the MPP.

To find the relationship between the voltage at MPP and the irradiance level, the P-V curves of the used PV module is plotted under irradiances from 100 W/m^2 to 1000 W/m^2 with a step of 100 W/m^2. All the irradiance levels and their corresponding MPP voltages are then imported into MATLAB, and the curve fitting tool *polyfit* is used to characterize the connection between them. In this paper, a 3rd-order polynomial is used. For the PV panel adopted, the obtained curve of V'_{mpp} versus irradiance intensity is expressed in (11). The total error of running curve fitting with a matching goodness-of-fit factor is below 0.042V. Fig. 5 shows the fitted curve. From Fig. 5, a cubic polynomial can well illustrate their dependence.

$$V'_{mpp} = 16.86S^3 - 37.97S^2 + 32.76S + 55.76 \quad (11)$$

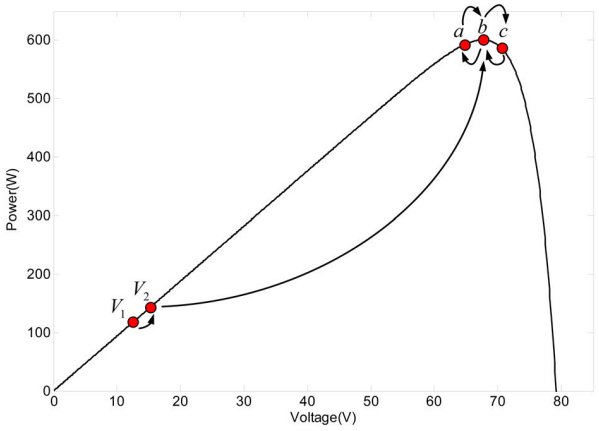

FIGURE 4. Diagram of operating scheme for the presented MPPT.

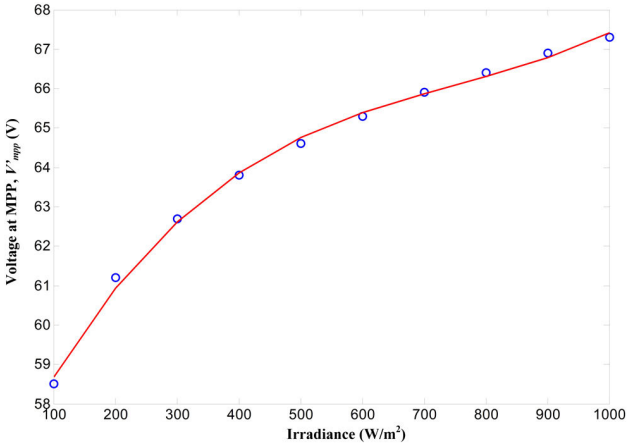

FIGURE 5. Fitted curve between the irradiance level and voltage at MPP.

It should be noted that the V'_{mpp} is not the voltage of true MPP because of the errors arising from the use of simplified PV model, SMSE, curve fitting, and measurement etc. However, it is very close to the voltage at true MPP provided that the irradiance is estimated correctly. Thus if the irradiance level is known, the V'_{mpp} can be obtained by substituting the irradiance value into (11). The flowchart of the proposed MPPT technique can be summarized as follows: Fig. 6 shows the operating process of the proposed MPPT algorithm. Firstly, the SMSE cycle, as described in subsection III.A, is utilized to estimate the irradiance level using two (V, I) samples. Once the irradiance level is known, the OVC can be calculated by substituting it into (11). In the second phase, the starting OP is moved to the obtained OVC and the α-P&O technique, as described in subsection III.B, is applied to take over the next tracking step. In α-P&O stage, the power change ΔP is utilized to determine whether an irradiance level change occurs ($\Delta P > \Delta P_{threshold}$) or not. If the irradiance level changes, two additional perturbation steps will be performed and the SMSE cycle will be run again to estimate the new irradiance and calculate the new OVC.

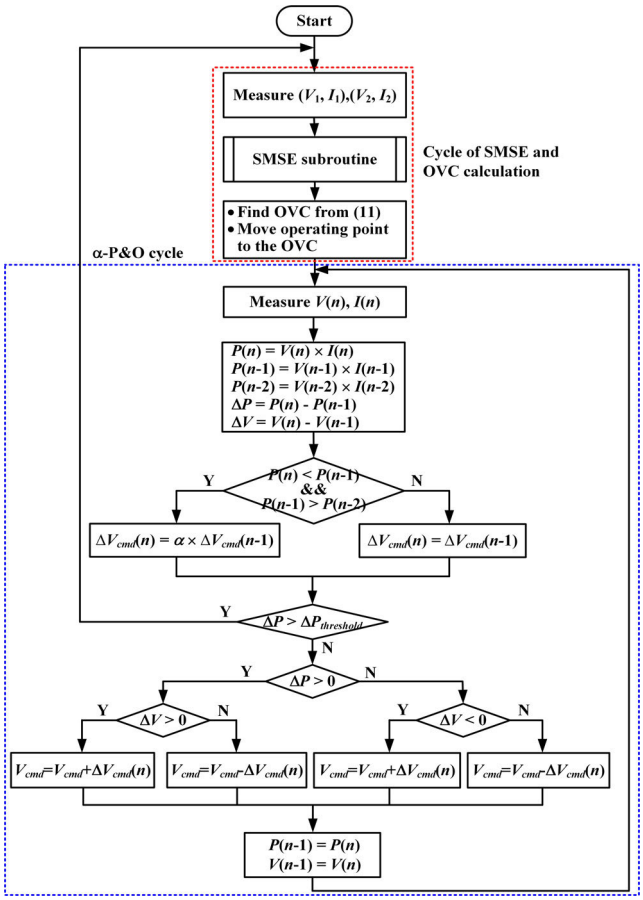

FIGURE 6. Operating flowchart of the presented MPPT.

IV. EXPERIMENTAL SYSTEM SETUP AND RESULTS

This section firstly introduces the system configuration, experimental setup, and indices of the performance evaluation. Next the correctness of the proposed MPPT algorithm are demonstrated experimentally. Finally, comparisons with previous methods under various testing scenarios are given to show the performance improvement of the proposed method.

A. CONFIGURATION & SETUP OF THE PROPOSED MPPT SYSTEM

Fig. 7 shows the configuration of the constructed 600W MPPT system. The PV modules are interfaced with a boost converter which serves as the MPP tracker to supply power to the load. A low-cost MCU dsPIC33FJ16GS502 from Microchip Corp. is used to implement the proposed MPPT algorithms and control the power switch of boost converter. The output voltage (V_T) and current (I_T) of the PV module are sampled and sent to the analog to digital converter (ADC). The noises involved in digitized data are filtered by the developed 32-order finite impulse response (FIR) digital filter which is programmed with the digital filter design tool from Microchip Technology Inc. [32]. The OVC (V_{cmd}) is obtained via the execution of the developed MPPT program. Based on the V_{cmd}, the duty cycle can be determined through the digital proportional integral differential (PID) compensator. Then

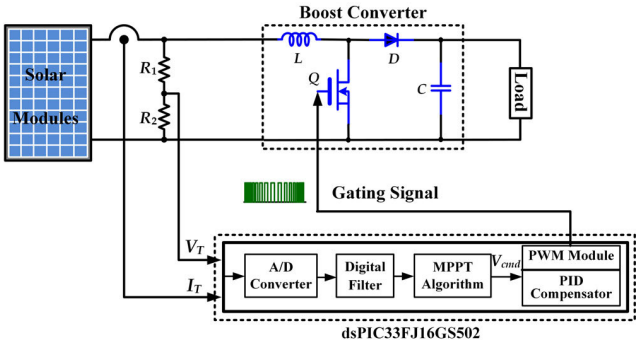

FIGURE 7. Configuration of the studied MPPT system.

TABLE 2. Specifications of employed PV modules.

Model	TYNS62610290	2S1P
Maximum Power P_{mpp}	290W	580W
Open-Circuit Voltage V_{OC}	39.54V	79.08V
Shot-Circuit Current I_{SC}	9.41A	9.41A
Maximum Power Voltage V_{mpp}	32.24V	64.48V
Maximum Power Current I_{mpp}	8.73A	8.73A

TABLE 3. Specifications and parameter design of boost converter.

Specification		Component Design	
Input Voltage	20-100V	Inductor L	1.08mH
Rated Output Voltage	200V	Capacitor C	100 μF
Rated Output Power	600W	MOSFET Q	IPP65R110CFDA
Switching Frequency	50kHz	Diode D	C3D10060
Output Voltage Ripple	1%		

the gating signal is outputted to regulate the boost converter. In this study, the adopted 2S1P PV modules is simulated by a solar array simulator (TerraSAS ETS 600 × 8 from AMETEK Inc.) and an electronic load (63108A from Chroma Inc.) is utilized as the system load. The specifications of the utilized PV module and the boost converter realized are listed in Tables 2 and 3, respectively.

B. PERFORMANCE EVALUATION INDEX (PEI)

To fairly evaluate and compare the test results of different MPPT methods, a performance evaluation index (PEI) is proposed in this study. Fig. 8 displays a schematic tracking response. The definition of each measured item illustrated in Fig. 8 is described as follows: 1) Rising time (t_r): time required for the tracking power reaches 95% of MPP; 2) Settling time (t_s): time required for the tracking power enters the range of ±1% of MPP; 3) Steady-state average power (P_{avg}): the sum of the power of 1s after steady state, and then divided by the acquired data numbers; 4) Steady-state tracking accuracy (ψ_{acc}): dividing the P_{avg} by the ideal MPP; 5) Tracking energy loss (E_{loss}): the gray area as shown in Fig. 8. It records the power for a preset duration and takes the absolute value of

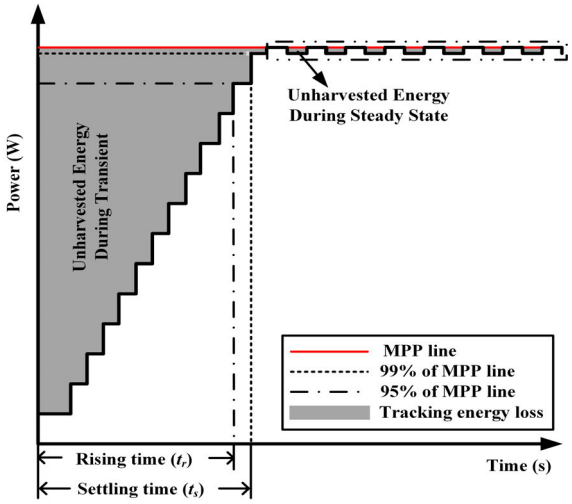

FIGURE 8. Tracking response of the MPPT operation.

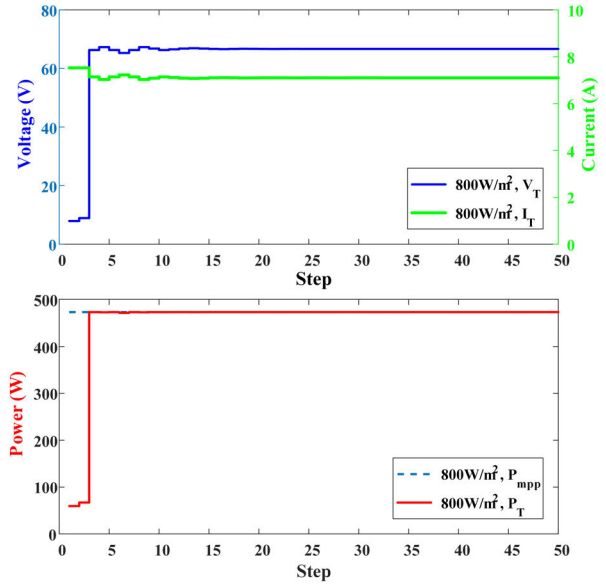

FIGURE 9. Simulated tracking curves under 800 W/m^2 and 298 K.

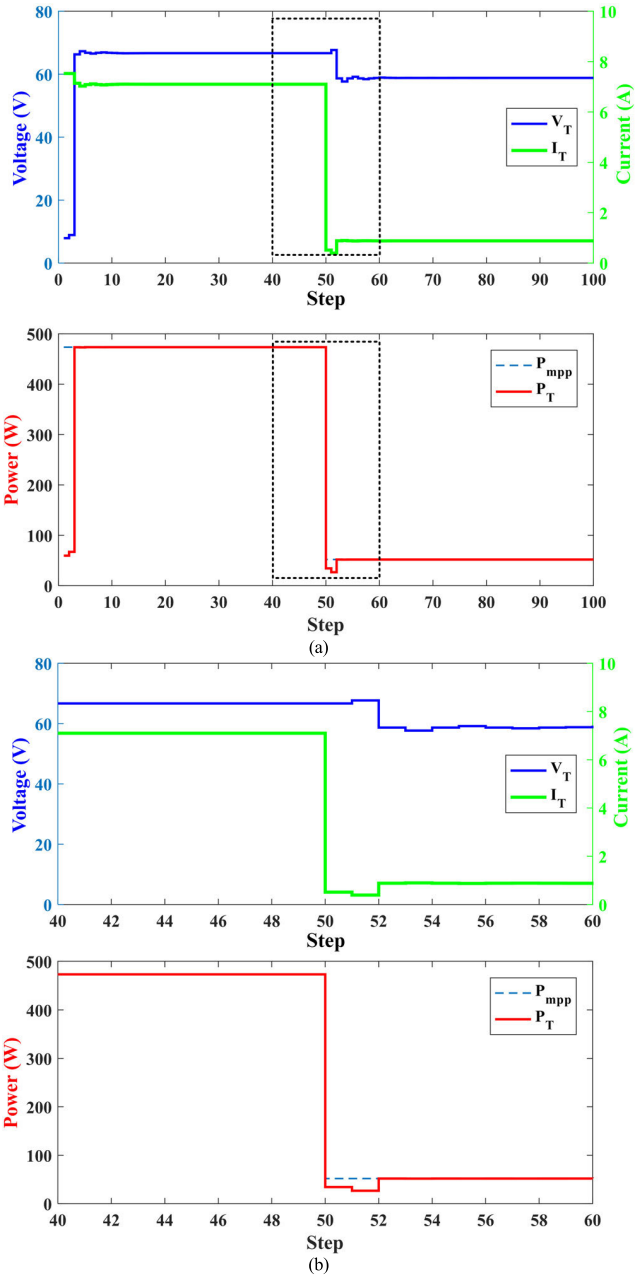

FIGURE 10. (a) Simulated tracking curves with irradiance change from 800 W/m^2 to 100 W/m^2 and 298 K. (b) Enlargement of the curve range selected in (a).

the tracking value minus the MPP value; 6) Average tracking power loss (P_{avg_loss}): E_{loss} divided by the preset duration.

C. SIMULATION RESULTS

In the simulation test, the OVC change is expressed by steps. The simulated tracking curves under 800 W/m^2 and 298 K for the proposed method were plotted in Fig. 9. The performance indices of the t_r, t_s, P_{avg}, ψ_{acc}, E_{loss}, and P_{avg_loss} were 0.6 s, 1.0 s, 463.95 W, 99.99 %, 823.6 J, and 16.5 W respectively. Besides, irradiance change scenario is also simulated to verify the tracking capability. Fig. 10(a) shows the tracking curves simulated under irradiance change from 800 W/m^2 to 100 W/m^2 and 298K. To more clearly observe the transients in power tracking, about 10 step range (as the selected dotted line range) before and after the irradiance change is enlarged as shown in Fig. 10(b). In Fig. 10(b), the irradiance change occurs at the 50th tracking step, after the irradiance change, only two measuring steps are needed to estimate the new irradiance level, and the α-P&O process is performed after moving the OP to the new OVC. Therefore, the MPP tracking of the proposed method is achieved rapidly and accurately.

D. EXPERIMENTAL RESULTS AND COMPARISONS

The setup of the experimental system was the same as that in simulation. The tracking command in the MPPT algorithm was updated every 0.2s. Fig. 11 illustrates the measured tracking waveforms of the proposed method under 800 W/m^2

TABLE 4. Summary of simulation and experimental results and performance comparison for three MPPT methods.

Method	FSS P&O (SS=3V)		VSS P&O (M=0.65)		Proposed		% [Red.(-)/Inc.(+)] vs. FSS P&O	% [Red.(-)/Inc.(+)] vs. VSS P&O
PEI	S^+	E^+	S^+	E^+	S^+	E^+	E^+	E^+
t_r (s)	3.8	3.9	2.4	2.5	0.6	0.6	-84.6 %	-76.0 %
t_s (s)	5.0	4.8	3.0	3.2	1.0	0.8	-83.3 %	-75.0 %
P_{avg} (W)	455.28	454.58	463.86	460.29	463.95	460.43	+1.26 %	+0.03 %
$_{acc}$ (%)	98.12	97.97	99.97	99.20	99.87	99.23	+1.26 %	+0.03 %
E_{loss} (J)	4277.4	4378.7	2577.4	2967.3	823.6	1403.3	-68.0 %	-52.7 %
P_{avg_loss} (W)	85.5	87.6	51.5	59.3	16.5	28.1	-67.9 %	-52.6 %

FSS: Fixed Step Size; VSS: Variable Step Size; P&O: Perturb and Observe; SS: Perturbation Step Size; M: Scaling Factor;
S^+: Simulated; E^+: Experimental (with solar array simulator) @800 W/m^2, 298K; Red.: Reduction; Inc.: Increase

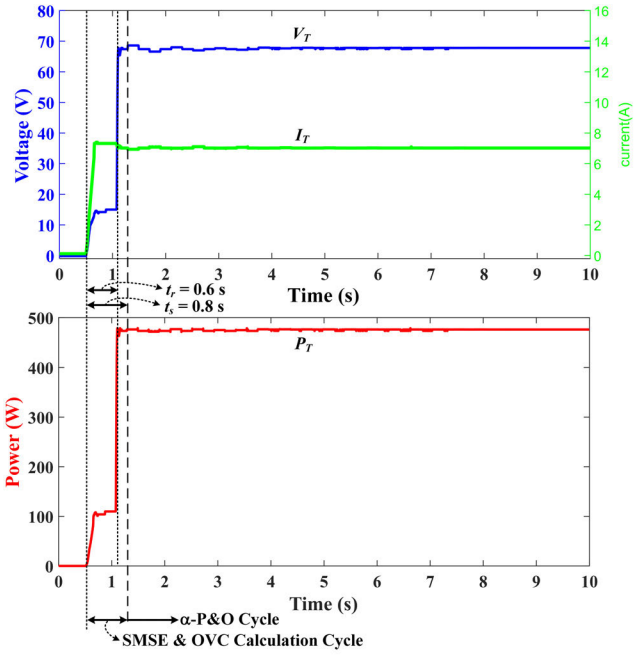

FIGURE 11. Measured tracking waveforms at 800 W/m^2 and 298K.

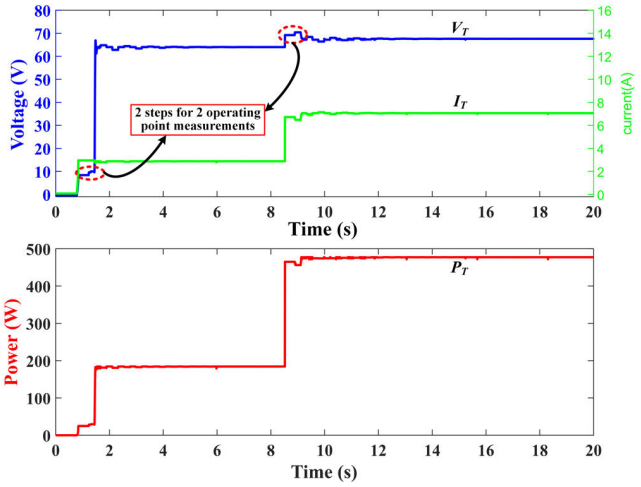

FIGURE 12. Measured waveforms with irradiance change from 300 to 800 W/m^2.

and 298 K. From the experimental results, the performance indices, t_r, t_s, P_{avg}, ψ_{acc}, E_{loss}, and P_{avg_loss}, were 0.6 s, 0.8 s, 460.43 W, 99.23 %, 1403.3 J, and 28.1 W, respectively. It is obvious that the SMSE and OVC calculation stage is performed firstly and then the α-P&O stage is executed afterward. Next, MPP tracking waveforms under sudden irradiance increase/decrease are measured and recorded. Fig. 12 shows the tracking waveforms of the irradiance change from 300 W/m^2 to 800 W/m^2 and 298 K. Relatively, the tracking waveforms of the irradiance change from 800 W/m^2 to 100 W/m^2 and 298 K were shown in Fig. 13. From Fig. 12 and 13, it can be seen that after the irradiance changes, only two OPs measurements are needed, next the algorithm will move the OVC to the vicinity of the MPP and then the α-P&O method is in charge of the subsequent tracking to reach the true MPP. These results correspond well with those in the simulations.

To further demonstrate the performance improvement of the proposed method, simulation and experimental results comparing with fixed step-size (FSS) P&O and variable step-size (VSS) P&O methods using the same prototyping circuit are summarized in Table 4. From Table 4, the difference between the simulated and the experimental results is small for all methods, so the correctness of the three realized MPPT methods is confirmed. From the experimental results, the FSS P&O indeed exists a trade-off problem, the t_r and ψ_{acc} cannot be optimized simultaneously because the SS is fixed. Hence, the t_r, t_s and ψ_{acc} of the FSS P&O are inferior to those of the other two. Although the VSS P&O can effectively deal with the trade-off problem of the FSS P&O, the design of an optimal scaling factor M is very challenging.

Experimental results have demonstrated that the proposed algorithm can improve the performances comparing with the other two methods. In terms of transient performance, the reductions in t_r are 3.3 s and 1.9 s, and the reductions in t_s are 4.0 s and 2.4 s, respectively. Consequently, compared with the FSS and VSS P&O methods, the tracking speed can be improved by 84.6 % and 76.0 %, respectively. In terms of steady state performance, the harvested P_{avg} and ψ_{acc} in FSS P&O are 454.58 W and 97.97 % respectively. The ψ_{acc} is unsatisfactory due to the power oscillation around the MPP after reaching steady state. Since the VSS P&O possesses the mechanism of step size variation, its ψ_{acc} increases to

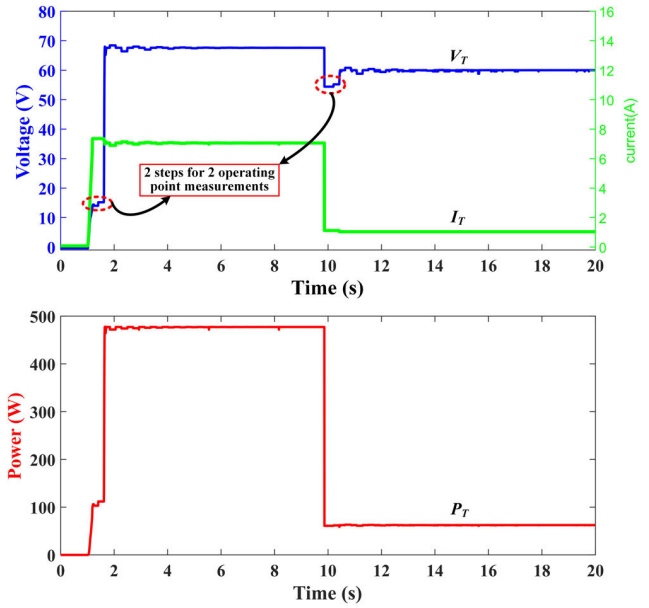

FIGURE 13. Measured waveforms with irradiance change from 800 to 100 W/m^2.

99.20 % and nearly no oscillations occur when it approaches the MPP. In this study, the α-P&O method is employed as the second stage, the obtained ψ_{acc} is 99.23 % which is better than that of the VSS P&O. Comparing with the FSS and VSS P&O techniques, the tracking accuracy can be improved by 1.26 % and 0.03 %, respectively. Regarding the tracking energy loss, the FSS P&O has the most E_{loss} during the MPP tracking due to the trade-off between transient and steady state performance. The VSS P&O owns better transient and steady-state responses, so the E_{loss} has a reduction of 32.2 % compared with the FSS P&O. The presented method has excellent transient and steady-state responses, so the E_{loss} is the lowest among the three methods. In summary, compared with FSS and VSS P&O methods, the E_{loss} has been improved by 68.0 % and 52.7 %, respectively.

V. CONCLUSION

A new swift MPPT algorithm combining two chasing stages for rapid irradiance changes has been proposed in this paper. Integrating the α-P&O technique with the simplified model-based state estimation, the complexity of computation and realization cost can be reduced significantly and make the usage of low-cost MCUs attainable. Simulated and experimental results show that tracking accuracies exceeds 99.2 % in all test scenarios, which confirm that the proposed algorithm has the capability to effectively harvest maximum energy during the MPPT. Comparing with the conventional FSS and VSS P&O methods, the tracking time is shortened by 84.6 % and 76.0 %, the tracking accuracy is improved by 1.26 % and 0.03 %, and the average tracking power loss is reduced by 68.0 % and 52.7 %, respectively. The proposed method features excellent dynamic response during the first stage and the oscillation power loss in steady state is significantly reduced in the second phase. The main contribution of this study is that the fast and accurate tracking can be achieved without the need of extra expensive irradiance and temperature sensors. The studied method is simple and can easily be integrated into conventional P&O algorithms, which makes the developed MPPT solution more suitable for industrial PGS applications. In addition, in the future work, the derivation and fitting of the relationship among the maximum power point voltage, irradiance, and temperature will be done, and then the critical parameters that affect the maximum power output of the PGS can be analyzed and discussed in detail to further improve the tracking technology and performance. The field test executed in the practical setup site will be performed also instead of the testing inside the lab using SAS to inspect the practical concept demonstration. On the other hand, at the current research stage, the limitation of the presented tracking method cannot manipulate the global maximum power tracking under partial shading conditions yet because the multiple peak values on the P-V curve will occur in different partial shading patterns. Therefore, the future work also will focus on finding the irradiance value of individual partially shaded area through the I-V characteristic curve to track the global maximum power point.

REFERENCES

[1] R. Rajesh and M. C. Mabel, "A comprehensive review of photovoltaic systems," *Renew. Sustain. Energy Rev.*, vol. 51, pp. 231–248, Nov. 2015.
[2] M. Obi and R. Bass, "Trends and challenges of grid-connected photovoltaic systems—A review," *Renew. Sustain. Energy Rev.*, vol. 58, pp. 1082–1094, May 2016.
[3] I. Houssamo, F. Locment, and M. Sechilariu, "Experimental analysis of impact of MPPT methods on energy efficiency for photovoltaic power systems," *Int. J. Electr. Power Energy Syst.*, vol. 46, pp. 98–107, Mar. 2013.
[4] M. A. Eltawil and Z. Zhao, "MPPT techniques for photovoltaic applications," *Renew. Sustain. Energy Rev.*, vol. 25, pp. 793–813, Sep. 2013.
[5] D. Verma, S. Nema, A. M. Shandilya, and S. K. Dash, "Maximum power point tracking (MPPT) techniques: Recapitulation in solar photovoltaic systems," *Renew. Sustain. Energy Rev.*, vol. 54, pp. 1018–1034, Feb. 2016.
[6] N. Kumar, B. Singh, and B. K. Panigrahi, "PNKLMF-based neural network control and learning-based HC MPPT technique for multiobjective grid integrated solar PV based distributed generating system," *IEEE Trans. Ind. Informat.*, vol. 15, no. 6, pp. 3732–3742, Jun. 2019.
[7] K. Sundareswaran, V. Vigneshkumar, P. Sankar, S. P. Simon, P. S. R. Nayak, and S. Palani, "Development of an improved P&O algorithm assisted through a colony of foraging ants for MPPT in PV system," *IEEE Trans. Ind. Informat.*, vol. 12, no. 1, pp. 187–200, Feb. 2016.
[8] S. K. Kollimalla and M. K. Mishra, "A novel adaptive P&O MPPT algorithm considering sudden changes in the irradiance," *IEEE Trans. Energy Convers.*, vol. 29, no. 3, pp. 602–610, Sep. 2014.
[9] F. Liu, S. Duan, F. Liu, B. Liu, and Y. Kang, "A variable step size INC MPPT method for PV systems," *IEEE Trans. Ind. Electron.*, vol. 55, no. 7, pp. 2622–2628, Jul. 2008.
[10] N. Karami, N. Moubayed, and R. Outbib, "General review and classification of different MPPT techniques," *Renew. Sustain. Energy Rev.*, vol. 68, pp. 1–18, Feb. 2017.
[11] S. K. Kollimalla and M. K. Mishra, "Variable perturbation size adaptive P&O MPPT algorithm for sudden changes in irradiance," *IEEE Trans. Sustain. Energy*, vol. 5, no. 3, pp. 718–728, Jul. 2014.
[12] K. S. Tey and S. Mekhilef, "Modified incremental conductance MPPT algorithm to mitigate inaccurate responses under fast-changing solar irradiation level," *Sol. Energy*, vol. 101, pp. 333–342, Mar. 2014.
[13] K. Sundareswaran, V. V. Kumar, and S. Palani, "Application of a combined particle swarm optimization and perturb and observe method for MPPT in PV systems under partial shading conditions," *Renew. Energy*, vol. 75, pp. 308–317, Mar. 2015.

[14] M. Kermadi, Z. Salam, J. Ahmed, and E. M. Berkouk, "An effective hybrid maximum power point tracker of photovoltaic arrays for complex partial shading conditions," *IEEE Trans. Ind. Electron.*, vol. 66, no. 9, pp. 6990–7000, Sep. 2019.
[15] N. Priyadarshi, S. Padmanaban, J. B. Holm-Nielsen, M. S. Bhaskar, and F. Azam, "Internet of Things augmented a novel PSO-employed modified zeta converter-based photovoltaic maximum power tracking system: Hardware realisation," *IET Power Electron.*, Jan. 31, 2020, doi: 10.1049/iet-pel.2019.1121.
[16] J.-H. Teng, W.-H. Huang, T.-A. Hsu, and C.-Y. Wang, "Novel and fast maximum power point tracking for photovoltaic generation," *IEEE Trans. Ind. Electron.*, vol. 63, no. 8, pp. 4955–4966, Aug. 2016.
[17] L. V. Hartmann, M. A. Vitorino, M. B. D. R. Correa, and A. M. N. Lima, "Combining model-based and heuristic techniques for fast tracking the maximum-power point of photovoltaic systems," *IEEE Trans. Power Electron.*, vol. 28, no. 6, pp. 2875–2885, Jun. 2013.
[18] L. Cristaldi, M. Faifer, M. Rossi, and S. Toscani, "An improved model-based maximum power point tracker for photovoltaic panels," *IEEE Trans. Instrum. Meas.*, vol. 63, no. 1, pp. 63–71, Jan. 2014.
[19] N. Priyadarshi, S. Padmanaban, P. K. Maroti, and A. Sharma, "An extensive practical investigation of FPSO-based MPPT for grid integrated PV system under variable operating conditions with anti-islanding protection," *IEEE Syst. J.*, vol. 13, no. 2, pp. 1861–1871, Jun. 2019.
[20] S. Padmanaban, N. Priyadarshi, J. B. Holm-Nielsen, M. S. Bhaskar, F. Azam, A. K. Sharma, and E. Hossain, "A novel modified sine-cosine optimized MPPT algorithm for grid integrated PV system under real operating conditions," *IEEE Access*, vol. 7, pp. 10467–10477, Jan. 2019.
[21] S. Padmanaban, N. Priyadarshi, M. S. Bhaskar, J. B. Holm-Nielsen, V. K. Ramachandaramurthy, and E. Hossain, "A hybrid ANFIS-ABC based MPPT controller for PV system with anti-islanding grid protection: Experimental realization," *IEEE Access*, vol. 7, pp. 103377–103389, Jul. 2019.
[22] N. Priyadarshi, S. Padmanaban, J. B. Holm-Nielsen, F. Blaabjerg, and M. S. Bhaskar, "An experimental estimation of hybrid ANFIS–PSO-based MPPT for PV grid integration under fluctuating sun irradiance," *IEEE Syst. J.*, vol. 14, no. 1, pp. 1218–1229, Mar. 2020.
[23] N. Priyadarshi, A. K. Sharma, and F. Azam, "A hybrid firefly-asymmetrical fuzzy logic controller based MPPT for PV-wind-fuel grid integration," *Int. J. Renew. Energy Res.*, vol. 7, no. 4, pp. 1546–1560, 2017.
[24] N. Priyadarshi, S. Padmanaban, M. S. Bhaskar, F. Blaabjerg, and A. Sharma, "Fuzzy SVPWM-based inverter control realisation of grid integrated photovoltaic-wind system with fuzzy particle swarm optimisation maximum power point tracking algorithm for a grid-connected PV/wind power generation system: Hardware implementation," *IET Electr. Power Appl.*, vol. 12, no. 7, pp. 962–971, Aug. 2018.
[25] S. Padmanaban, N. Priyadarshi, M. S. Bhaskar, J. B. Holm-Nielsen, E. Hossain, and F. Azam, "A hybrid photovoltaic-fuel cell for grid integration with Jaya-based maximum power point tracking: Experimental performance evaluation," *IEEE Access*, vol. 7, pp. 82978–82990, Jun. 2019.
[26] N. Priyadarshi, S. Padmanaban, M. S. Bhaskar, F. Blaabjerg, J. B. Holm-Nielsen, F. Azam, and A. K. Sharma, "A hybrid photovoltaic-fuel cell-based single-stage grid integration with Lyapunov control scheme," *IEEE Syst. J.*, early access, Nov. 18, 2020, doi: 10.1109/JSYST.2019.2948899.
[27] N. Priyadarshi, S. Padmanaban, L. Mihet-Popa, F. Blaabjerg, and F. Azam, "Maximum power point tracking for brushless DC motor-driven photovoltaic pumping systems using a hybrid ANFIS-FLOWER pollination optimization algorithm," *Energies*, vol. 11, no. 5, pp. 1–16, Apr. 2018.
[28] N. Priyadarshi, M. S. Bhaskar, S. Padmanaban, F. Blaabjerg, and F. Azam, "New CUK–SEPIC converter based photovoltaic power system with hybrid GSA–PSO algorithm employing MPPT for water pumping applications," *IET Power Electron.*, early access, Jan. 31, 2020, doi: 10.1049/iet-pel.2019.1154.
[29] M. G. Villalva, J. R. Gazoli, and E. R. Filho, "Comprehensive approach to modeling and simulation of photovoltaic arrays," *IEEE Trans. Power Electron.*, vol. 24, no. 5, pp. 1198–1208, May 2009.
[30] M. E. Baran and A. W. Kelley, "State estimation for real-time monitoring of distribution systems," *IEEE Trans. Power Syst.*, vol. 9, no. 3, pp. 1601–1609, Aug. 1994.
[31] Y.-H. Liu, J.-H. Chen, and J.-W. Huang, "Global maximum power point tracking algorithm for PV systems operating under partially shaded conditions using the segmentation search method," *Sol. Energy*, vol. 103, pp. 350–363, May 2014.
[32] B. K. A. Ramu, "Implementing FIR and IIR digital filters using PIC18 microcontrollers," Microchip Technol., Chandler, AZ, USA, Appl. Note AN852, 2002.

SHUN-CHUNG WANG received the Ph.D. degree in electrical engineering from National Taiwan University, Taipei, Taiwan, in 1995. He is currently with the Department of Electrical Engineering, Lunghwa University of Science and Technology, Taoyuan, Taiwan. His current research interests include power electronics, and energy conversion control and their applications.

HUNG-YU PAI was born in Changhua, Taiwan, in 1997. He received the B.S. degree in electrical engineering from the National Taiwan University of Science and Technology, in 2019, where he is currently pursuing the Ph.D. degree with the Department of Electrical Engineering. His research interests include power electronics, Li-ion battery charging algorithm, and Li-ion battery SOC estimation algorithm.

GUAN-JHU CHEN (Student Member, IEEE) was born in Taichung, Taiwan, in 1990. He received the B.S. degree in electrical engineering from Kun Shan University, in 2012, and the M.S. degree in electrical engineering from the National Taiwan University of Science and Technology (NTUST), in 2014, where he is currently pursuing the Ph.D. degree with the Department of Electrical Engineering. His research interests include power electronics, digital power control, and Li-ion battery charging algorithm.

YI-HWA LIU (Member, IEEE) received the Ph.D. degree in electrical engineering from National Taiwan University, Taipei, Taiwan, in 1998. He joined the Department of Electrical Engineering, Chang Gung University, Taoyuan, Taiwan, in 2003. He is currently with the Department of Electrical Engineering, National Taiwan University of Science and Technology, Taipei. His current research interests include power electronics and battery management.